Design and detailed analysis of a scanning tunnelling microscope

1990 Meas. Sci. Technol. 1 139

(http://iopscience.iop.org/0957-0233/1/2/007)

Meas. Sci. Technol. 1 (1990) 139–146. Printed in the UK

Design and detailed analysis of a scanning tunnelling microscope

S Grafström, J Kowalski and R Neumann

Physikalisches Institut der Universität Heidelberg, Philosophenweg 12, D-6900 Heidelberg, FRG

Received 27 February 1989, in final form 23 June 1989, accepted for publication 15 August 1989

Abstract. A scanning tunnelling microscope (STM) is described which uses a double-lever reduction system with a single micrometer-drive for the coarse sample-to-tip approach and a thermally compensated single-tube piezo scanner for the tip movement. The microscope is equipped with versatile analogue electronics, and the data acquisition is computer-automated. The principal considerations are two main problems in the design of the STM electronics: the current control circuit and the current-sensing preamplifier. The performance of the STM is illustrated with images of gold and graphite samples.

1. Introduction

Since its invention, scanning tunnelling microscopy (Binnig *et al* 1982, Binnig and Rohrer 1986, Hansma and Tersoff 1987) has developed into a widely used technique for surface studies, rendering atomic resolution in vacuum as well as in air or liquids. In the present paper we describe a scanning tunnelling microscope (STM) comprising an easy-to-handle and reliable mechanical arrangement of novel design for the coarse sample approach towards the tunnelling tip, a thermally compensated piezoelectric scanner assembly and versatile electronic equipment for the tunnelling current control. Besides a detailed description of our set-up and its performance, we present some more general considerations of interest for STM design. The microscope is depicted in figure 1. The photograph visualises several important parts, namely the tube piezo which carries the tunnelling tip facing the sample, the double-lever mechanism for the sample movement mounted on a vibration-isolating plate stack, and the housing containing the tunnelling current preamplifier.

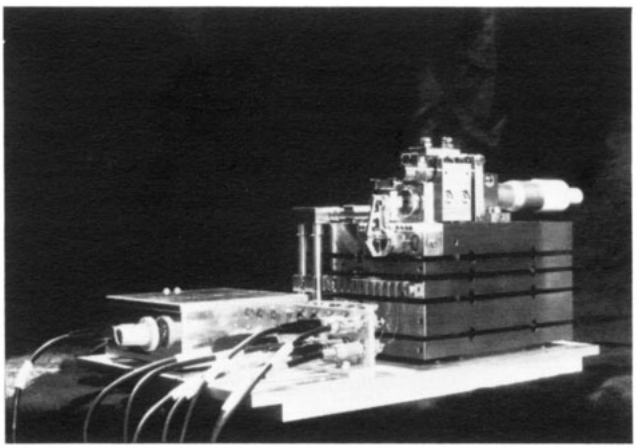

Figure 1. Photograph of the STM.

2. Mechanical set-up

2.1. Sample movement

Four top views of the mechanical set-up are shown in figure 2. They illustrate the macroscopic sample approach to the tunnelling tip. Similar to the design of Demuth *et al* (1986a,b) both sample rotation and linear motion are effected with a single micrometer screw but in a somewhat different way. The sample holder (A) is mounted on a hardened steel rod (B) sliding without backlash between six fixed steel balls in a stainless steel frame (C). This frame and the lever denoted D are both pivoting around a common perpendicular axis (E). D is connected via springs to rod B. A second lever (F) sits on axis G. Frame C and levers D and F are all loaded by coiled springs. The motion of the micrometer screw H is transmitted by lever F to lever D, and from there to frame C in the case of sample rotation, and to rod B in the case of linear sample movement.

The approach procedure is divided into three stages. In figure 2(*a*) the sample is turned away from the tip by $\sim 51°$. This position provides good access to sample and tip, necessary for exchange and transfer. During stage 1 the sample is turned via retraction of the micrometer shaft until frame C hits stop I, the rotation thus coming to an end, and the sample now facing the tip at a distance of about 3.1 mm. In stage 2 (figure 2(*b*)) the sample propagates 3 mm towards the tip with a 1:1 transmission from micrometer to sample, lever D pushing rod B forward in frame C. When the position of figure 2(*c*) is reached, a 1:100 reduction becomes effective (stage 3, figure 2(*d*)), the two levers (1:5 and 1:20) now acting as a

0957-0233/90/020139 + 08 $03.50

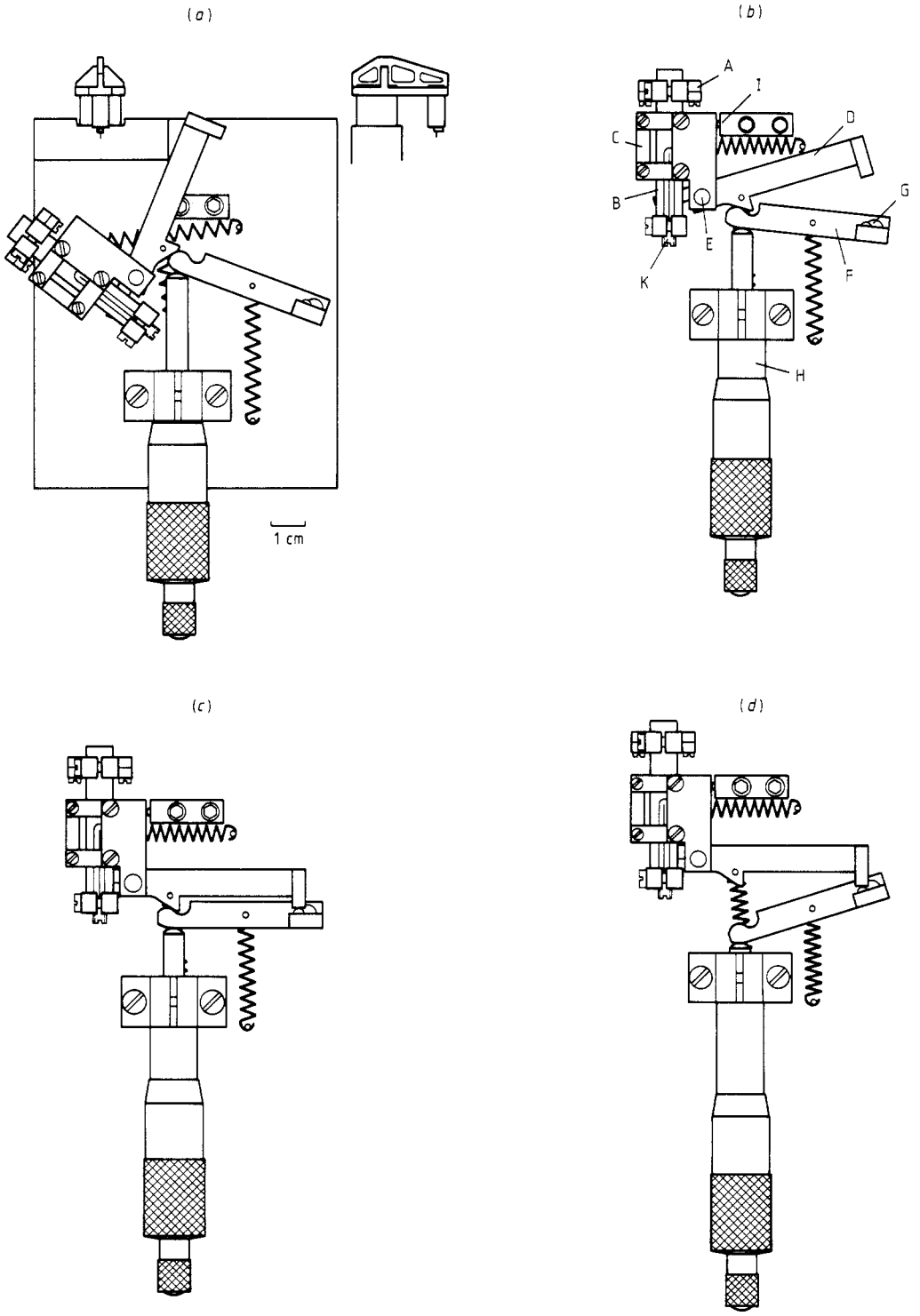

Figure 2. Schematic top view of the lever mechanism for sample movement, comprising four stages. (*a*) Sample turned away from the tip by ~51°. (*b*) Sample propagates linearly towards the tip with a 1:1 transmission. (*c*) The position where a 1:100 reduction becomes effective. (*d*) The two levers acting as one 'folded' lever. See text for details.

'folded' lever. Stage 3 allows a well defined feed of 0.14 mm with 5 μm per micrometer screw revolution. The tip-to-sample distance in the position where the mechanism switches from stage 2 to stage 3 must be preadjusted with screw K to lie within the travel range of stage 3. In contrast to other systems with lever reduction, the sample is not tilted during the approach towards the tip. The sample is mounted in a small cylindrical case screwed to the sample holder A. This allows fast sample exchange without renewed preadjustment. The electric connection between the sample and the preamplifier is established automatically at the end of stage 1. The lateral position of the sample relative to the tip can be adjusted within a ± 1 mm range by changing the position of the stop I with a screw, thus slightly turning the sample. The whole microscope is fabricated mainly from stainless steel in order to allow its future use in ultra-high vacuum with minor modifications only.

2.2. Piezo scanner

We use a single-tube scanner (Binnig and Smith 1986) providing a good combination of stiffness and high sensitivity. The tube, fabricated from P1 88 piezo ceramics (Quartz & Silice, France), has an outer diameter of 5 mm, a wall thickness of 0.5 mm and an active length of 9 mm. Its outer electrode is divided into four segments. Voltages with opposite polarities are applied to opposite electrodes, allowing bending of the tube in the x and y directions. The inner electrode is used for the longitudinal (z) movement. The tunnelling tip is clamped with a small screw in a tiny stainless steel holder ($1.6 \times 2 \times 2.8\ \text{mm}^3$) glued to the tube with a Macor sheet in between, and sits symmetrically on the tube axis in order to obtain the lowest possible cross-coupling between lateral and longitudinal movement.

The bending of the scanner piezo was calibrated by deflecting a laser beam with a small mirror glued to the piezo tube and by detecting its displacement with a quadrant photodiode. The diode position signal was calibrated by measuring the signal change resulting from a well defined lateral displacement of the diode. The x and y sensitivity of the piezo scanner was thus found to be $11\ \text{nm V}^{-1}$, taking into account that the tip is protruding about 4 mm beyond the tube end. The stated value was later very well confirmed by the STM images taken of graphite with its well known lattice constant. The z calibration was performed with a Michelson interferometer and yielded a value of $\sim 3.8\ \text{nm V}^{-1}$. We use low voltages of ± 12.7 V, resulting in a total x, y range of $\sim 280 \times 280\ \text{nm}^2$ and a z travel of ~ 96 nm which is sufficient for many applications. We thus avoid the necessity of fast low-noise high-voltage amplifiers and connected problems like capacitive coupling of high-voltage noise to tip or sample. With these low voltages the linearity is good with a hysteresis of a few per cent only.

The scanner is combined with a second tube piezo (outer diameter 12 mm, wall thickness 1.3 mm) in parallel arrangement (see inset in figure 2(a)), which is driven with voltages of ± 300 V giving a travel of $\sim 1.5\ \mu$m in the z direction. This piezo is used to facilitate a safe approach of the sample towards the tip and normally acts as a slow feedback element in the tunnelling current control circuit (see § 3.3). Moreover, it provides thermal compensation of the tube scanner in the z direction. The two tubes are connected with each other through a light and rigid stainless steel frame to which they are glued with 'Torr Seal' epoxy resin (Varian, Italy). The rest of the microscope is also fabricated from stainless steel so there should be no thermal drift in the x, y plane if all parts are subject to equal temperature changes. The lowest resonant frequency of the scanner assembly is ~ 5.3 kHz which – possibly due to the glue – is lower than estimated from the involved masses and elastic constants, and the geometry.

2.3. Vibration isolation

A stack of four stainless steel plates serves for vibration isolation of the microscope (Gerber *et al* 1986). Each plate lies on three cylindrical Viton spacers acting as resilient and damping elements. As expected from theoretical calculations based on experimental results of Okano *et al* (1987) concerning spring and damping constants of Viton rubber, the stack should exhibit a transfer function (defined as the ratio of the vibration amplitude of the top plate to that of the ground) for vertical vibrations with a pronounced resonance at about 15 Hz, little isolation between ~ 30 Hz and ~ 100 Hz, and a steep roll-off above 100 Hz. Since the Viton elements are standing upright, lateral forces cause bending of the elements. Therefore, the stack is rather soft in the horizontal plane, and lateral vibrations are assumed to be isolated somewhat better than vertical ones. For improved isolation of lower frequencies, the STM set-up is placed on a heavy stone bench lying on air tubes. A box with sound-absorbing glass wool walls ensures efficient acoustic shielding. One can probably improve the isolation capability of the stack by replacing the lower plates by a larger number of thinner plates without increasing the overall size. Besides a steeper roll-off above 100 Hz, this will also give a somewhat improved isolation down to ~ 15 Hz.

3. STM electronics

3.1. Feedback loop analysis

Theoretical considerations concerning the current control circuit of the STM have been published by Pohl (1986) and Park and Quate (1987a). Here we start from the discussion by Pohl assuming that the feedback loop consists of the tunnelling junction with its exponential dependence of current on gap width s, a logarithmic amplifier for linearisation, an integrator and the piezo actuator. Then a change δs of s produces a proportional signal change $\delta U = K\delta s$ at the output of the logarithmic amplifier. We assume that the frequency response of the loop is dominated by the integrator and the piezo element, their transfer functions being

$$F_{\mathrm{I}}(\mathrm{i}\omega) = 1/\mathrm{i}\omega\tau$$

and

$$F_{\mathrm{P}}(\mathrm{i}\omega) = \frac{a_0}{1-(\omega/\omega_{\mathrm{r}})^2 + \mathrm{i}(\omega/\omega_{\mathrm{r}})(1/Q)}$$

respectively where $\omega = 2\pi\nu$, ν is the frequency, τ the integrator time constant, a_0 the piezo sensitivity (nm V^{-1}) for zero frequency, $\omega_{\mathrm{r}} = 2\pi\nu_{\mathrm{r}}$, ν_{r} is the piezo resonant frequency, Q the quality factor and $\mathrm{i} = \sqrt{-1}$. For simplification we describe the piezo element by a single mechanical resonance. The complex open-loop gain now reads

$$F_{\mathrm{Loop}}(\mathrm{i}\omega) = KF_{\mathrm{I}}(\mathrm{i}\omega)F_{\mathrm{P}}(\mathrm{i}\omega).$$

The feedback loop is stable if $F_{\mathrm{Loop}}(\mathrm{i}\omega)$, plotted as a curve in the complex plane (Nyquist diagram, figure 3), does not enclose the critical point -1 but passes to the right of it. For sufficient stability one normally demands a phase margin of 45° and an amplitude margin of 8 dB (Ebel

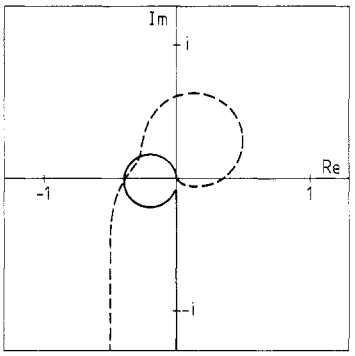

Figure 3. Nyquist diagram of the STM feedback loop without (full curve) and with (broken curve) additional low-pass filter.

1982), i.e. the phase should be at least 45° away from −180° at the frequency where the gain drops below 1 (unity gain frequency), and the gain should be at least 8 dB below 1 at the frequency where the phase shift is −180°. For the feedback loop considered this latter point occurs exactly at the resonant frequency ν_r where the gain exhibits a peak. Consequently, the time constant τ has to be chosen large enough to depress this peak sufficiently below 1 which gives the Nyquist diagram displayed in figure 3 (full curve, $Q = 10$). Figure 4 shows the corresponding Bode diagram with the absolute value $G = |F_{\text{Loop}}(i\omega)|$ and the phase $\varphi(i\omega)$ as functions of the frequency ($\nu_r = 5$ kHz in our example).

As pointed out by Pohl (1986), one can add a higher-order low-pass filter in order to speed up the feedback loop. This filter has two effects:

(i) The resonant peak is somewhat damped in amplitude.

(ii) The more important feature is the occurrence of an additional phase lag which – with a proper choice of filter type and cut-off frequency – shifts the point with $\varphi = -180°$ to a frequency near the minimum of $|F_{\text{Loop}}(i\omega)|$ at $\nu < \nu_r$ (see Bode diagram, figure 4, broken curve). One can then decrease the time constant τ, thereby increasing the unity gain frequency to about $\nu_r/5$ without infringing upon the amplitude margin of 8 dB. In the Nyquist diagram the resonance is thus rotated away from the critical point −1 (figure 3, broken curve). In our example we use a second-order Butterworth low-pass with a cut-off frequency of $0.6\ \nu_r = 3$ kHz.

With the knowledge of the loop gain $F_{\text{Loop}}(i\omega)$ one is able to calculate the step response of the closed feedback loop (Ebel 1982) which was done by a computer using an inverse fast Fourier transform (FFT) algorithm. Figure 5 shows how the loop returns back to equilibrium after a step-like disturbance in the two cases considered above. The improvement obtained by the low-pass filter is evident, the settling time being lowered to about $2.5/\nu_r = 0.5$ ms. If Q is rather small, as turned out to be the case for our present scanner, the improvement is not so noticeable. In reality, there are of course always several elements within the feedback loop causing additional phase shifts, the most important in many cases being the preamplifier. However, their cut-off frequencies are often too high to produce the required phase lag, so a further adjustable low-pass filter of first or second order will be suitable for optimisation of the circuit. It can also help damp the higher resonances that were neglected in our discussion.

3.2. Preamplifier

As common, a current-to-voltage converter, based on an operational amplifier (op-amp), is used as a preamplifier, giving an output voltage $U = -RI$ with an input current I and a feedback resistor R (figure 6). Desired features are low noise and wide bandwidth. When R is large ($R \geqslant 1$ MΩ), thermal resistor noise (Johnson noise) will be a main contribution to the amplifier noise, provided that a low-noise op-amp is used:

$$U_{\text{therm}} = \sqrt{4kTR\Delta f}$$

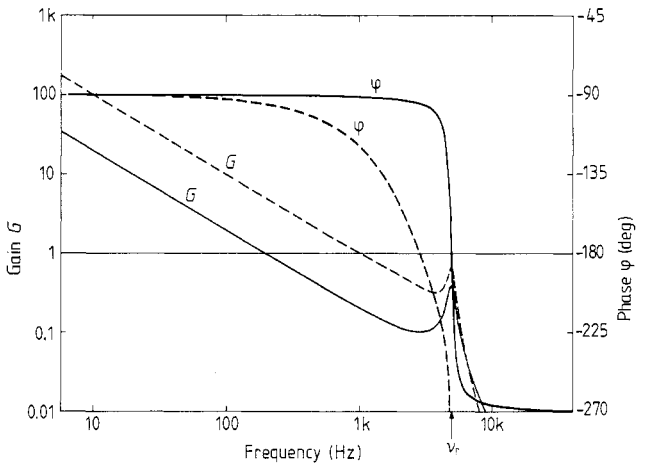

Figure 4. Bode diagram of the STM feedback loop without (full curve) and with (broken curve) additional low-pass filter.

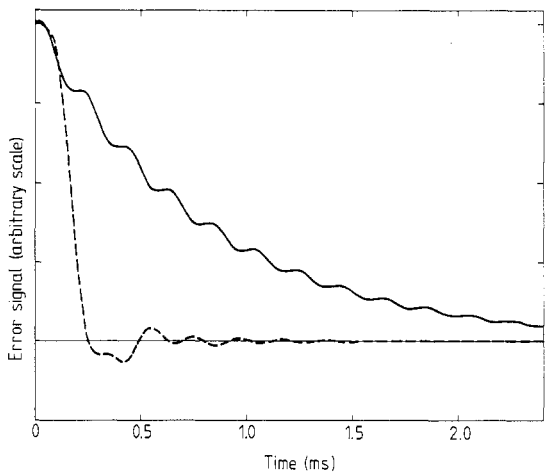

Figure 5. Step response of the closed STM feedback loop without (full curve) and with (broken curve) additional low-pass filter.

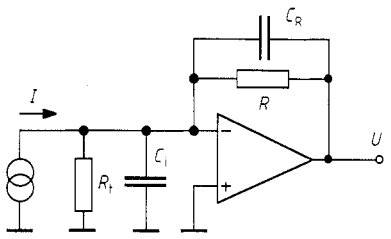

Figure 6. Circuit diagram of current-to-voltage converter (I = current, R_t = source resistance, C_i = input capacitance, R = feedback resistance, C_R = feedback capacitance, U = output voltage).

k being Boltzmann's constant, T the absolute temperature and Δf the bandwidth. This contribution may be compared with the shot noise of the current I, which generates a voltage noise at the amplifier output and yields a lower limit to the total noise:

$$U_{\text{shot}} = R\sqrt{2Ie\Delta f}$$

where e is the electron charge. To approach this theoretical limit as closely as possible, R should be chosen so large that $U_{\text{therm}} < U_{\text{shot}}$ which gives the condition $R > 50\ \text{mV}/I$ at room temperature. For example, a typical tunnelling current of 1 nA requires $R > 50\ \text{M}\Omega$. It should be pointed out that especially in air tunnelling current noise clearly exceeds pure shot noise (Abraham *et al* 1988, Tiedje *et al* 1988). Therefore, the above value provides only a rough guide for selecting R. In conclusion, R should lie in the range of 1 MΩ–1 GΩ to give good signal-to-noise ratio for tunnelling currents from 10 pA to 100 nA.

To estimate the available bandwidth one has mainly to consider the influence of the input capacitance C_i. C_i has a destabilising effect by causing a phase lag of the voltage fed back via R to the amplifier input. This phase shift has to be compensated for by putting a capacitor C_R parallel to R. The loop gain of this configuration is given by (Tietze and Schenk 1986)

$$v(\omega) = v_0(\omega)\frac{Z_1(\omega)}{Z_1(\omega) + Z_2(\omega)}$$

$v_0(\omega)$ being the op-amp's open-loop gain.

$$Z_1 = R_t \| 1/i\omega C_i \qquad \text{and} \qquad Z_2 = R \| 1/i\omega C_R$$

are the impedances at the amplifier input and in the feedback path respectively. R_t is the current source resistance, and in our case corresponds to the tunnelling resistance. Taking R_t much larger than R which is the most critical case concerning stability, and assuming $C_i \gg C_R$, the above expression yields

$$v(\omega) = v_0(\omega)\frac{1 + i\omega RC_R}{1 + i\omega RC_i}.$$

We assume a unity-gain stable op-amp with an open-loop gain exhibiting a -20 dB/decade roll-off. By analysing $v(\omega)$, one then finds that a phase margin of $\gtrsim 50°$ requires

$$C_R > C_i/\sqrt{2\pi f_T RC_i}$$

or the equivalent condition

$$f_c = \frac{1}{2\pi RC_R} < \frac{1}{2\pi}\left(\frac{2\pi f_T}{RC_i}\right)^{1/2}$$

where f_T is the unity gain frequency of the operational amplifier ($|v_0(2\pi f_T)| = 1$). For a phase margin of 65°, C_R has to be a factor of $\sqrt{2}$ larger. f_c is an approximate value for the cut-off frequency of the low-pass current-to-voltage converter. The above formula, which holds as long as $\sqrt{2\pi f_T RC_i} \gg 1$, expresses the importance of choosing an operational amplifier with high f_T and of keeping the input capacitance low in order to obtain the highest possible bandwidth. The op-amp should, of course, also have a small bias current I_B to be suitable for measuring small currents. For high values of $R(\gtrsim 100\ \text{M}\Omega)$ the bandwidth will in practice often be limited by the intrinsic shunt capacitance of R. Figure 7(*a*) shows the response of such an amplifier to a δ-pulse as calculated by an inverse Fourier transform of the theoretical amplifier frequency response with $R = 100\ \text{M}\Omega$, $C_i = 20$ pF and $C_R = 0.08$ pF for two different values of f_T, thus illustrating the influence of f_T. For comparison, figures 7(*b*) and (*c*) display experimental scope traces produced by coupling a voltage step to the amplifier input via a capacitor. The experimental parameters were about the same as those used in the calculation. Integration of the δ-pulse response yields the step response.

We use either an OPA 602 or an OPA 606 op-amp (Burr Brown) with $f_T = 6.4$ MHz, $I_B = 0.5$ pA and $f_T = 13$ MHz, $I_B = 5$ pA respectively. They are fitted with switchable resistors of 1, 10, 100 and 1000 MΩ. The input capacitance consists of wiring capacitance, the capacitance of the switch used to select R, and the op-amp's own input capacitance. Where possible, C_R was adjusted to give optimum step response with no or only minor overshoot of a few per cent with $C_i \approx 20$ pF. Thus, bandwidths ranging from 2 to 300 kHz are obtained, depending on R and on the op-amp used. With $R = 100\ \text{M}\Omega$ the 3 dB bandwidth is 18 kHz for the OPA 602 and 25 kHz for the OPA 606 with rise times of 19 μs and 13 μs respectively. For comparison, $R = 10\ \text{M}\Omega$ gives bandwidths of about 73 and 100 kHz, and rise times of 5 and 3.7 μs respectively. Bandwidth and step response were checked by using a biased low-capacitance photodiode illuminated by a light-emitting diode as a signal source.

3.3. Electronic design

The electronics of the tunnelling current control circuit is displayed in figure 8. The general design is similar to that described by other authors (Park and Quate 1987b), but many details are different. The preamplifier converts the tunnelling current into a proportional voltage (see § 3.2). It is located close to the STM in order to keep the input capacitance low. Sample and amplifier are connected via a low-capacitance coaxial line, consisting of a thin copper wire (⌀ 0.1 mm) in a stainless steel tube (inner diameter 4 mm). After optional further amplification, the signal is

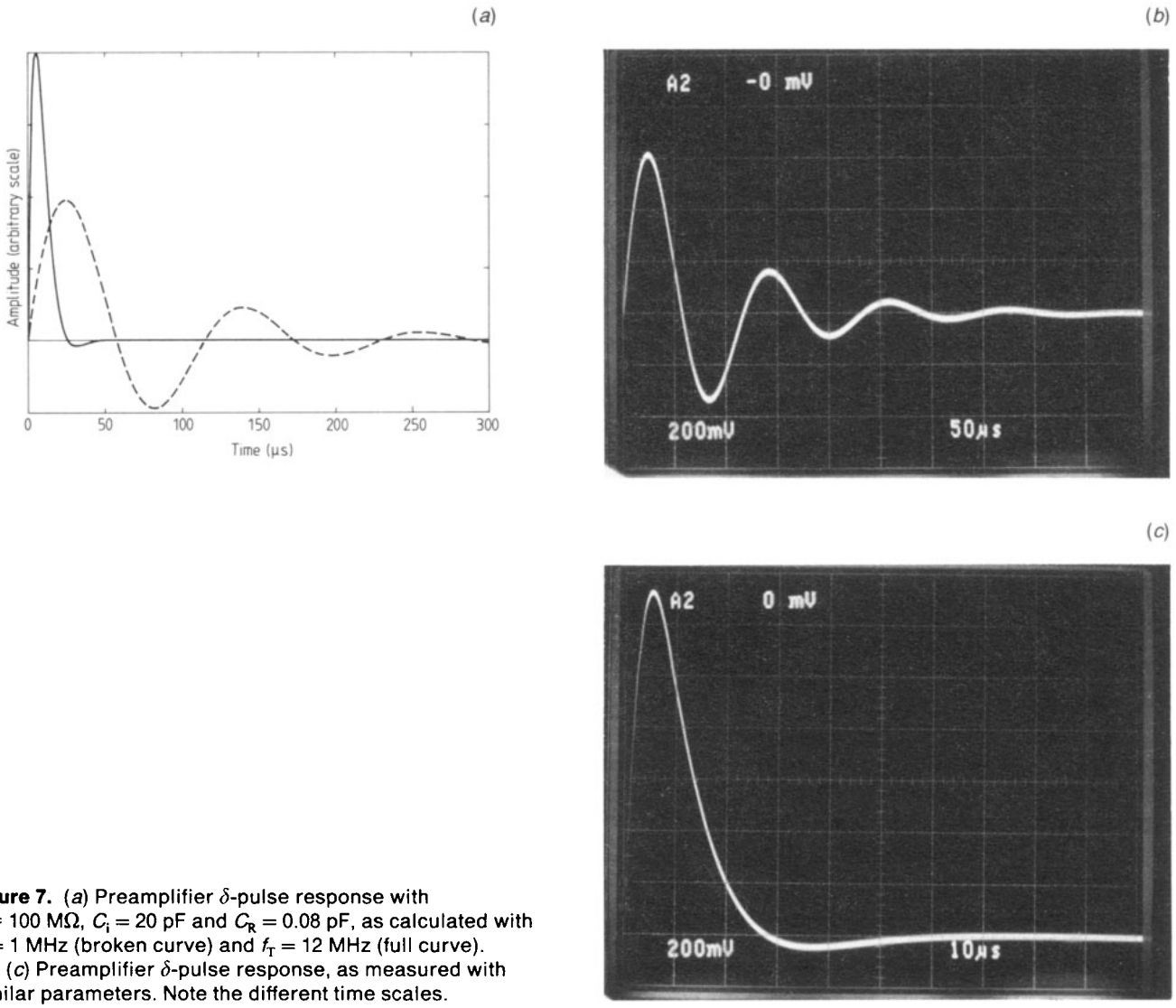

Figure 7. (*a*) Preamplifier δ-pulse response with $R = 100$ MΩ, $C_i = 20$ pF and $C_R = 0.08$ pF, as calculated with $f_T = 1$ MHz (broken curve) and $f_T = 12$ MHz (full curve). (*b*), (*c*) Preamplifier δ-pulse response, as measured with similar parameters. Note the different time scales.

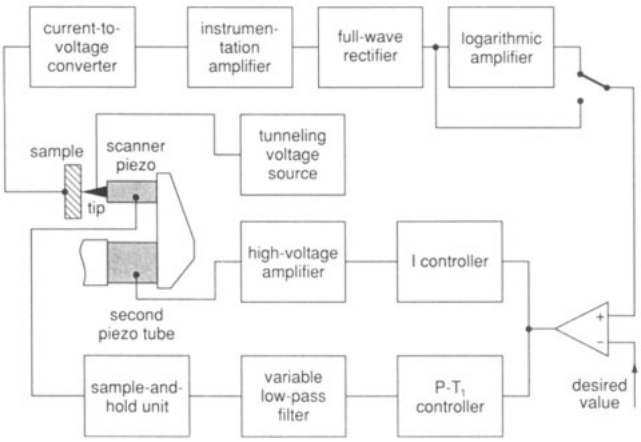

Figure 8. STM current control circuit. In the constant-current mode, the *z* signal on the scanner piezo is used for imaging, whereas in the constant-height mode a signal proportional to the tunnelling current or its logarithm is used.

rectified so that the feedback loop is not affected by a polarity reverse of the tunnelling voltage. An optional log-amplifier can be used to linearise the exponential dependence of tunnelling current on sample-to-tip distance. Subtraction of the desired value yields the error signal which serves as input for two controllers working in parallel: a P–T_1 and an I controller (Ebel 1982). The P–T_1 controller is a proportional amplifier followed by a low-pass filter. It exhibits P behaviour (constant gain) below the low-pass cut-off frequency ν_c and integral behaviour (gain ~ 1/frequency) well above ν_c, and operates as a fast feedback element acting on the inner electrode of the scanner piezo. The I controller is an integrator with a larger time constant and acts on the second tube piezo through a high-voltage amplifier of simple design (± 300 V, 4 kHz bandwidth, < 5 mV peak-to-peak noise). For low frequencies the gain of the I branch dominates, but drops below that of the P–T_1 branch for higher frequencies. Therefore, the I branch averages only slow drifts of the sample-to-tip distance, whereas the P–T_1 branch provides the fast feedback signal used for imaging in the constant-current mode. The feedback loop is actuated automatically when the tunnelling current surpasses a preset level.

The control unit can also be easily used in configurations other than the one described, for example by

activating only one controller, or by summing both controller outputs and feeding them to the same piezo element. The integrator time constant can be set continuously from 1 ms to 10 s. The P–T_1 module allows independent setting of gain (six levels between 2 and 100) and of unity gain frequency (continuously). When increasing the gain, the cut-off frequency ν_c of the low-pass is lowered at the same time by the appropriate amount to keep the unity gain frequency ν_1 constant. Proper selection of ν_1 is decisive for settling time and stability of the feedback circuit, so it is very convenient not to have its setting altered when changing the gain. The available regime of the time constant

$$\tau' = 1/2\pi\nu_1 = \tau/v$$

covers the range from 0.1 to 100 ms, $\tau = (2\pi\nu_c)^{-1}$ being the time constant of the low-pass filter and v the gain of the proportional amplifier. In addition to the controllers, a further optional low-pass filter can be inserted into the signal path in order to speed up the feedback circuit according to the circuit analysis (see § 3.1). It can be operated as a low-pass of first or second order, alternatively with critical damping, or with Bessel or Butterworth characteristics, with a cut-off frequency between about 1 and 100 kHz.

For acquiring I/V spectra with the CITS technique (Hamers *et al* 1986) the feedback loop can be gated. For this purpose both the integrator (I controller) and the low-pass filter of the P–T_1 controller serve as sample-and-hold units. During the hold mode the signal path is interrupted by low-leakage analogue switches, and the capacitors of integrator and RC low-pass store their respective voltages. In the P–T_1 branch an additional integrated sample-and-hold circuit can be used to diminish sample-to-hold offset error and droop rate. In this case the hold capability of the P–T_1 controller prevents excessive sudden voltage changes on the piezo when switching back from hold to sample mode. With the controllers connected in the way described above, the droop rate during the hold mode amounts to $< 0.05\ \text{nm s}^{-1}$ and the sample-to-hold offset error is < 0.005 nm under typical conditions.

For control of the piezo scanner two analogue input signals for x and y in the range of ± 10 V are low-pass filtered with adjustable time constants (to smooth the voltage steps from the DACs and thus prevent oscillations of the tip), optionally attenuated, and fed to four output stages. These stages provide, with a small amplification, the output signals $+x$, $-x$, $+y$, $-y$ in the range of ± 12.7 V. Cross-coupling between x and y due to imperfections of the piezo tube can be cancelled electronically by mixing part of the y signal to the x signal. A further input for each channel (x, y) allows addition of a modulation voltage for acquisition of differential images (Abraham *et al* 1988) or for tracking tunnelling microscopy (Pohl and Möller 1988).

Three monitor outputs provide switch-selectable access to all important analogue signals of the feedback loop. One of these outputs is also connected to a digital display. Incorporated into the electronics is a signal conditioner with two channels offering several options: ± 10 V offset range, high-pass filtering (0.3 Hz–1 kHz), wide-bandwidth amplification ($\times 1$–100) and low-pass filtering (0.03–100 kHz). It is used for conditioning of signals recorded by the computer or by other means.

4. Computer automation

The microscope is controlled by a computer (Euromak C, Dr Weiss GmbH, FRG), equipped with an 8 bit microprocessor (Motorola 6809) and 56 kbyte of random access memory. The main program providing the user interface and supervising all functions is written in BASIC. Several programs written in assembly language do all time-critical tasks like scanning, data acquisition and on-line monitoring. Two 12 bit DACs are used to generate the raster scan, and a 12 bit ADC with 25 μs conversion time digitises the data. The highest possible scan speed is about 80 μs per raster point. The image is monitored on-line as a series of line scans or as a 3 bit colour map on a screen. Hard copies are produced with a colour pen plotter, and the data can be stored on floppy disc. The image size is restricted to 80×80 raster points due to the limited memory available. Because of this severe drawback and other disadvantages the present computer will be replaced by a Macintosh II in the near future.

5. Performance

So far, the STM has been tested in ambient air at room temperature with graphite and gold samples. Tips are produced either by electrochemical etching of tungsten wire ($\varnothing$ 0.25 mm) in 2M NaOH using alternating current, or by mechanical sharpening of Pt/Ir wire ($\varnothing$ 0.25 mm). The Pt/Ir tips are cleaned with acetone. They often produce the better pictures, whereas the tungsten tips often seem to be contaminated, probably by an oxide layer (Biegelsen *et al* 1987). STM pictures can be taken in the constant-current, the constant-height (Bryant *et al* 1986) and the differential (Abraham *et al* 1988) imaging modes. The shortest achievable settling time of the feedback loop is about 0.4 ms and is limited by the lowest scanner resonance of 5.3 kHz. It is difficult to specify the z stability, since the tunnelling current noise is often dominated by contributions other than vibrational perturbations when operating the microscope in air (Park and Quate 1986, Tiedje *et al* 1988). However, we estimate the short-time z stability to be about 0.01 nm under the present operating conditions. The long-time stability was checked by repeatedly scanning a pronounced feature of a gold surface. The two images shown in figure 9 are 46.6 min apart in time. The reproducibility of the imaged structure appears to be very good. The average lateral drift amounted to about $0.2\ \text{nm min}^{-1}$ and occurred almost exclusively in the y direction. The z drift as measured during the same run was about $0.15\ \text{nm min}^{-1}$ and is assumed to be mainly due to some mismatch of thermal expansion between the

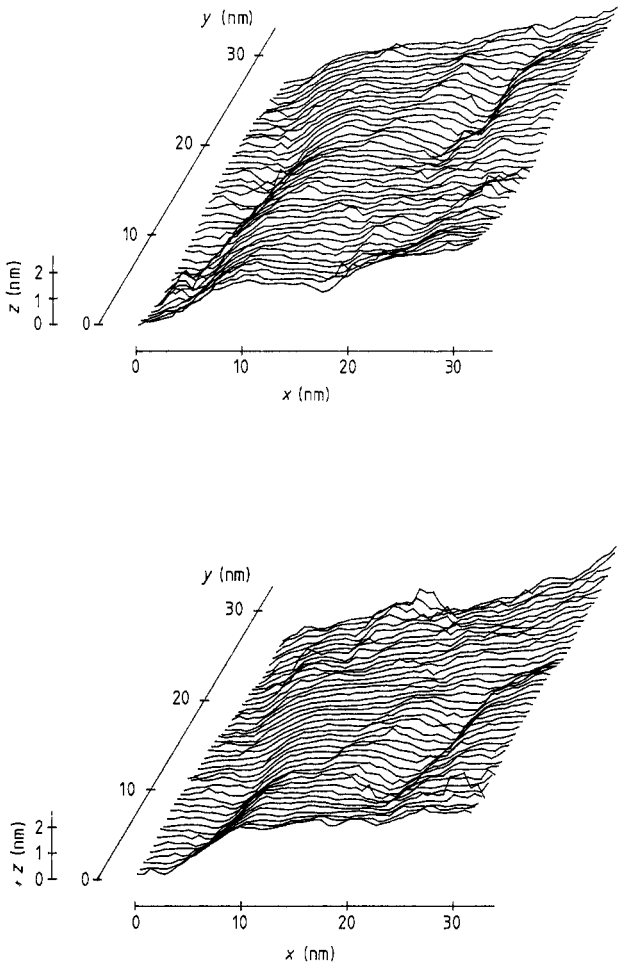

Figure 9. Constant-current images of a gold surface, 46.6 min apart in time. The tunnelling current was 1 nA with the tip at −1 V.

rod which carries the sample holder and the rest of the microscope. Therefore, some improvement should be possible with a better choice of material for the rod or with thermal compensation. The y drift could be due to mechanical creep rather than thermal drift. Figure 10 exemplifies atomic resolution, displaying an image of highly oriented pyrolytic graphite obtained in the constant-height mode with an acquisition time of 1 s. The average current was 3 nA, the tip voltage being

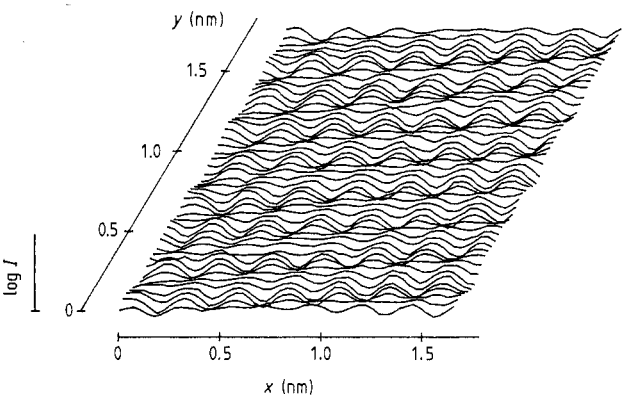

Figure 10. Constant-height image of highly oriented pyrolytic graphite.

−100 mV. The current variations amount to about 1 nA. The picture exhibits a clear distortion-free hexagonal lattice of depressions which are identified as the hollow sites within the carbon hexagons (Batra *et al* 1987).

Acknowledgments

The skilful support of our workshops for fine mechanics and electronics is gratefully acknowledged. We thank S Noehte for photographic documentation.

References

Abraham D W, Williams C C and Wickramasinghe H K 1988 Noise reduction technique for scanning tunneling microscopy *Appl. Phys. Lett.* **53** 1503–5

Batra I P, García N, Rohrer H, Salemink H, Stoll E and Ciraci S 1987 A study of graphite surface with STM and electronic structure calculations *Surf. Sci.* **181** 126–38

Biegelsen D K, Ponce F A, Tramontana J C and Koch S M 1987 Ion milled tips for scanning tunneling microscopy *Appl. Phys. Lett.* **50** 696–8

Binnig G and Rohrer H 1986 Scanning tunneling microscopy *IBM J. Res. Dev.* **30** 355–69

Binnig G, Rohrer H, Gerber Ch and Weibel E 1982 Tunneling through a controllable vacuum gap *Appl. Phys. Lett.* **40** 178–80

Binnig G and Smith D P E 1986 Single-tube three-dimensional scanner for scanning tunneling microscopy *Rev. Sci. Instrum.* **57** 1688–9

Bryant A, Smith D P E and Quate C F 1986 Imaging in real time with the tunneling microscope *Appl. Phys. Lett.* **48** 832–4

Demuth J E, Hamers R J, Tromp R M and Welland M E 1986a A simplified scanning tunneling microscope for surface science studies *J. Vac. Sci. Technol.* A **4** 1320–3

—— 1986b A scanning tunneling microscope for surface science studies *IBM J. Res. Dev.* **30** 396–402

Ebel T 1982 *Regelungstechnik* (Stuttgart: Teubner)

Gerber Ch, Binnig G, Fuchs H, Marti O and Rohrer H 1986 Scanning tunneling microscope combined with a scanning electron microscope *Rev. Sci. Instrum.* **57** 221–4

Hamers R J, Tromp R M and Demuth J E 1986 Surface electronic structure of Si(111)-(7 × 7) resolved in real space *Phys. Rev. Lett.* **56** 1972–5

Hansma P K and Tersoff J 1987 Scanning tunneling microscopy *J. Appl. Phys.* **61** R1–R23

Okano M, Kajimura K, Wakiyama S, Sakai F, Mizutani W and Ono M 1987 Vibration isolation for scanning tunneling microscopy *J. Vac. Sci. Technol.* A **5** 3313–20

Park S and Quate C F 1986 Tunneling microscopy of graphite in air *Appl. Phys. Lett.* **48** 112–4

—— 1987a Theories of the feedback and vibration isolation systems for the scanning tunneling microscope *Rev. Sci. Instrum.* **58** 2004–9

—— 1987b Scanning tunneling microscope *Rev. Sci. Instrum.* **58** 2010–7

Pohl D W 1986 Some design criteria in scanning tunneling microscopy *IBM J. Res. Dev.* **30** 417–27

Pohl D W and Möller R 1988 "Tracking" tunneling microscopy *Rev. Sci. Instrum.* **59** 840–2

Tiedje T, Varon J, Deckman H and Stokes J 1988 Tip contamination effects in ambient pressure scanning tunneling microscopy imaging of graphite *J. Vac. Sci. Technol.* A **6** 372–5

Tietze U and Schenk Ch 1986 *Halbleiterschaltungstechnik* (Berlin: Springer)